Int. J. Electrochem. Sci., 9 **(2014)** 3279 - 3286

International Journal of
ELECTROCHEMICAL
SCIENCE
www.electrochemsci.org

Short Coummunication

Synthesis and Lithium Storage Properties of Li-Mn-O compounds: Crystal Growth of $LiMn_2O_4$ and Li_2MnO_3

Bingjing Li[*], *Zheng Dang, Yong Zhang, Zhansong Song*

Mining Products Safety Approval and Certification Center, Beijing, 100013, PR China
[*]E-mail: zimubingjing@sina.com

Received: 14 January 2014 / *Accepted:* 19 February 2014 / *Published:* 23 March 2014

The present work describes using γ-MnOOH nanorods as a self-template to form Li-Mn-O compounds via hydrothermal process and state reaction, and a key finding in phase transition from cubic to monoclinic with Li content increasing. As the cathode material for lithium batteries, the electrochemical performances of as-prepared materials are investigated.

Keywords: MnOOH; Li-Mn-O; Cathode materials; Lithium-ion battery; Storage properties.

1. INTRODUCTION

Rechargeable lithium ion batteries have a wide range of applications from portable electronics, power tools, and electric vehicles.[1-3] Nanostructuring battery materials have emerged as an attractive method for further enhancing the battery performance.[4] Li-Mn-O system has attracted considerable attention as a cathode material due to its high power density, low cost, environmental friendliness, and high abundance.[5-7] However, developing various methods fully fabricate a certain substance such as $LiMn_2O_4$ and $LiMnO_2$, it is essential to investigate interior phase transitions of the Li-Mn-O system.

In the Li-Mn-O system, three types of compounds had been prepared by a conventional solid state reaction technique[8]: (1) the cubic $LixMn_{1-x}O$ phase with $x<0.35$ is abbreviated as 'c-MnO', (2) the orthorhombic $Li_{1/2}Mn_{1/2}O$ as 'o-$LiMnO_2$' and (3) the monoclinic $Li_{2/3}Mn_{1/3}O$ as 'm- Li_2MnO_3', respectively. The 'c-MnO' with $x<0.35$ exhibits a disordered cubic NaCl-type structure of space group Fm3m.[9] The 'o-$LiMnO_2$' is an orthorhombic variation of the NaCl structure with Li^+ and Mn^{3+} ions ordered (Pmnm).[10] The 'm-Li_2MnO_3' is a monoclinic variation of the NaCl-type superstructure with ordering of the layers of Li^+ ions and the layers of Li^+ and Mn^{4+} ions (C2/m).[11] From the formulas

analysis, the crystal structure of $Li_xMn_{1-x}O$ may be changed from 'c-MnO' (x<0.35, Fm3m) via 'o-$LiMnO_2$' (Pmnm) to 'm-Li_2MnO_3' (C2/m) as x increases. Therefore, the Li content is considered as an independent parameter for controlling the structural and physical properties of Li-Mn-O compounds.

Herein, Li-Mn-O compounds are successfully fabricated via solid state reaction using γ-MnOOH nanorods as a selftemplate. The phase transition and the electrochemical lithium storage of Li-Mn-O nanocomposites are investigated.

2. EXPERIMENTAL

Experiment details were as follows: 0.084 g $MnSO_4 \cdot H_2O$ and 0.474 g $KMnO_4$ were mixed well in a 32 mL distilled water and then a quantitative amount of CTAB was added as surfactant under vigorously stirred for 30 min. Afterwards, the turbid suspension was transferred into a 50 mL Teflon-lined stainless-steel autoclave, sealed, and maintained at 160 ºC for 25 h. After the reaction completed, the resulted brown solid products were centrifugalized, washed with deionized water and ethanol to remove the ions possibly remaining in the final product, and finally dried at 60 °C in air. The γ-MnOOH synthesized was thoroughly mixed with $LiOH \cdot H_2O$ beforeheating. The mixture placed in a porcelain crucible was calcinated at 550 ºC for 15 h in a Muffle furnace in air, then cooled to room temperature naturally. The precipitation was filtered and washed with ethanol. The solid product was vacuum-dried at 60 ºC for 10 h. The runs were carried out varying two parameters: the LiOH content and the γ-MnOOH. The molar ratio ([Li]/[Mn]) in the mixture were 1:1, 1.5:1, 2:1, respectively.

Crystal structural analysis of the synthesized materials were examined by X-ray diffraction (XRD; Cu Kα radiation) while the particle morphology, size and distribution were characterized by scanning electron microscopy (SEM) and transmission electron microscopy (TEM). Powder sample was mixed with KBr and pressed into pellets for Fourier transformed infrared (FTIR) analysis on AVATAR spectrometer between 4000 and 400cm^{-1}. The electrodes were fabricated from 75:10:15 (wt.%) mixture of active material: polyvinylidene difluoride (PVDF) as a binder: carbon black as a conducting agent. The testing half-cells of both kinds of electrodes were assembled in an Ar filled glove box (MB-10-G with TP170b/mono, MBRAUN) with a Li sheet as a counter and reference electrode. Electrolyte was 1M $LiPF_6$ in a mixed solution of EC and DEC (1:1 in volume ratio). The charge-discharge measurements were galvanostatically carried out in a battery test system (NEWARE BTS-610, Newware Technology Co., Ltd., China) at a constant current density.

3. RESULTS AND DISCUSSION

All of the XRD peaks in the Figure 1a can be readily indexed to a monoclinic phase of γ-MnOOH with lattice constants a=5.300Å, b=5.278Å and c=5.307Å, compatible with the literature values of JCPDS No.41-1379. No characteristic peaks of impurity phases are present in the Figure 1a, indicating the high purity of the final products. Figure 1b displays the FTIR spectra of sample γ-MnOOH. Two broad peaks at 3440 and 1630 cm^{-1} occur in the spectra, which are due to a small

amount of absorbed water in the sample. The peaks at 1085, 1119 and 1152cm^{-1} were attributed to the OH-bending modes, respectively to γ-OH, -2-OH and -1-OH.[12] The broad peak at 2600–2700 cm^{-1} is the fundamental O–H stretching bands related to the hydrogen band, with an O–H…O length of ~2.60 A in the structure of manganite. The peak at 2083 cm^{-1} is interpreted as the combination of the OH stretching mode at 2682 cm^{-1} and the excited lattice mode at 592 cm^{-1}, i.e. 2680−592=2088 cm^{-1}. This value is very close to what Kohler et al.[13] have reported. The sharp peaks at 446, 488, 592 and 646 cm^{-1} are attributed to the vibrations of the Mn–O bonds in γ-MnOOH. The FTIR spectra was consistent with typical reported references aboutγ-MnOOH.[14] The morphology of γ-MnOOH by the hydrothermal process assisted with CTAB is shown in Figure 1c. The γ-MnOOH crystallites are nanorods with anaverage diameter of 200-300 nm and tens of microns in length. The rod-like nanostructure of the sample is further examined by TEM, shown in Figure 1d. It indicates its single-crystalline structure, corresponding selected area electron diffraction (SAED) pattern. The diffraction spots can be indexed to (11-1), (020) and (1-31) planes of monoclinic γ-MnOOH (JCPDS No.41-1379).

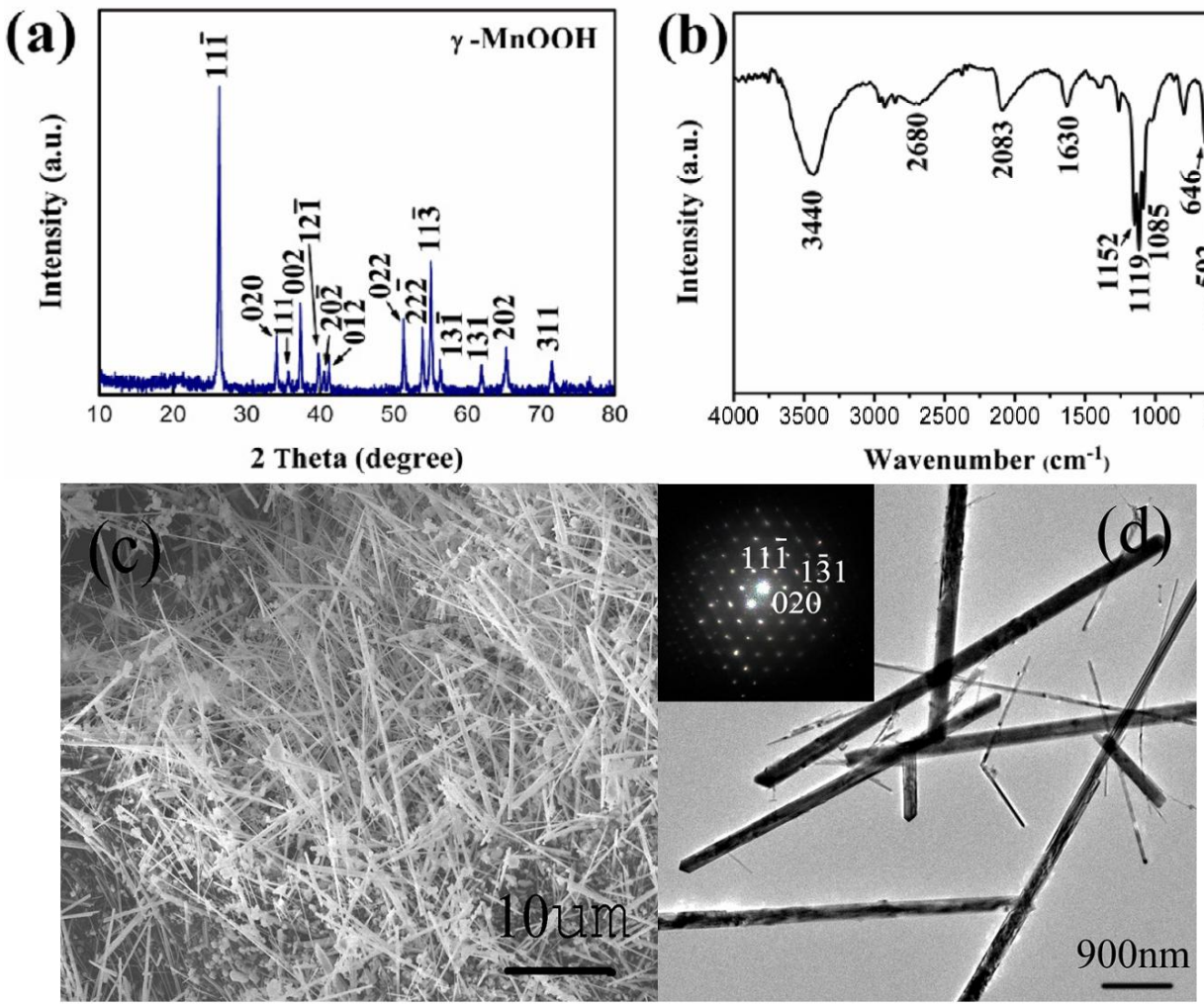

Figure 1. (a) XRD pattern, (b) FTIR spectra, (c) SEM image, (d) TEM image of the as-synthesized γ-MnOOH nanorods, (insets) corresponding SAED patterns.

Figure 2 displays the XRD patterns of as-prepared samples. Sample A synthesized at 550 ºC for 15 h, with Li/Mn ratio equal to 1:1, consists of pure phase of $LiMn_2O_4$ (curve a in Fig,2). It shows the feature of the spinel structure with cubic phase (Fd3m, space group 227, JCPDS data No.35-0782). No peaks of the γ-MnOOH precursor phase and other impurities were detected even though the sample was synthesized at a relatively lower temperature than typical reaction temperature of spinel $LiMn_2O_4$. [15] Curve b gives the XRD pattern of sample B which Li/Mn ratio is equal to 1.5:1. The obtained sample was composed of the mixture of $LiMn_2O_4$ and Li_2MnO_3 (JCPDS card No. 27-1252). It shows that the reaction was not complete and the intermediate product was $LiMn_2O_4$. As the Li content increased, the diffraction peaks were quite sharper due to the high crystallinity of the Li2MnO3 powder. Well developed peaks in all synthesized materials at 2θ =64.5^o and 65.5^o corresponds (108) and (110) directions clearly remained, which indicated the degree of development of the monoclinic structure of Li_2MnO_3. It was evident that the low-intensity ordering peaks at 2θ degree of 21-23° (arrowed in curve b, c) was the characteristic of a Li_2MnO_3-type structure with $LiMn_6$ (or Ni-substituted) cation arrangements in the transition metal layers.[16] When we heated γ-MnOOH nanorods with $Li(OH)\cdot H_2O$ at 550 ºC for 15 h, the molar ratio ([Li]/[Mn]) was 2:1, the XRD result indicated that a pure Li_2MnO_3 in curve c. All of the materials were indexed as a Li_2MnO_3 monoclinic structure with a space group of C2/m, which structure is the same as that of R3m layered rock-salt structures. Those experiment illustrated the crystal structure of Li-Mn-O can be changed from $LiMn_2O_4$ (Fd3m) to Li_2MnO_3 (C2/m) as Li content increases. Moreover, figure 3 shows the Rietveld refinement patterns for the Sample A and Sample C. The lattice parameters are listed in Table 1.

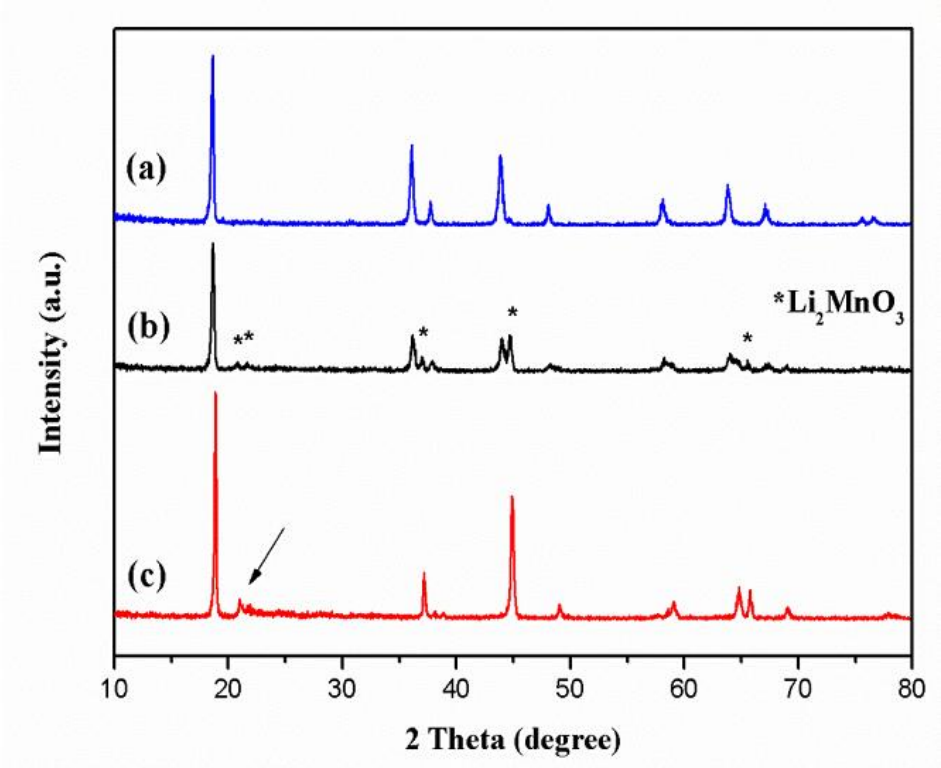

Figure 2. XRD patterns of as-prepared samples. The molar ratio [Li]/[Mn] is equal to (a) 1:1, (b)1.5:1, (c) 2:1, respectively.

Table 1. The lattice parameters of $LiMn_2O_4$ and Li_2MnO_3 obtained been synthesized via a template-sintered reaction using γ-MnOOH nanorods as a template.

	a	b	c	V	α	β	γ
$LiMn_2O_4$	8.243	8.243	8.243	560.285	90.000	90.000	90.000
Li_2MnO_3	4.937	8.530	5.023	199.681	90.000	109.284	90.000

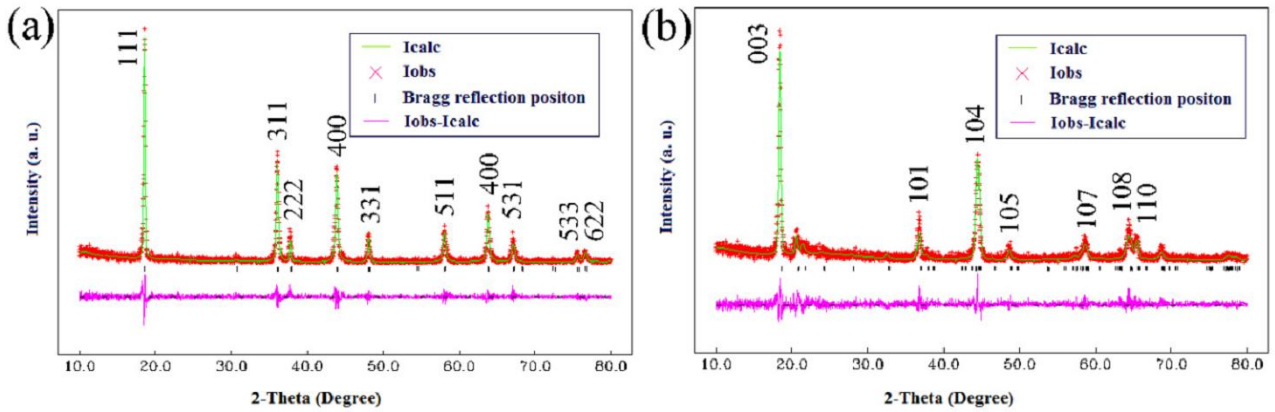

Figure 3. The Rietvelt refinement pattern for the samples obtained by solid state reaction using γ-MnOOH rods as a self-template. (a) $LiMn_2O_4$, (b) Li_2MnO_3.

The SEM images (Figure 4a and b) show that two samples have similar rods morphology with the width of 300-400 nm and the length of 500nm- 5μm. All the samples were well dispersed and maintained the morphology of γ-MnOOH nanorods self-template after an irreversible phase transition, only that rods became shorter in length. It is probably ascribed to the high-temperature process/damage. It can be also observed that the rods of Li_2MnO_3 is relatively uniform, however, $LiMn_2O_4$ rods have some cracks and slight agglomeration.

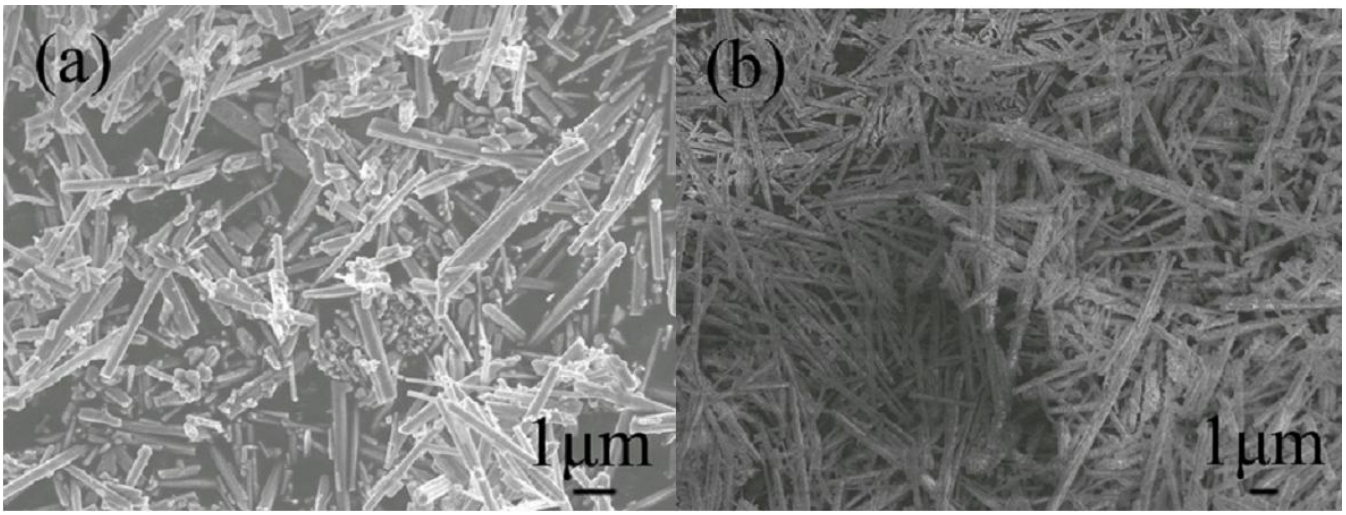

Figure 4. SEM images of the samples obtained at varying Li/Mn ratio: (a) $LiMn_2O_4$; (b) Li_2MnO_3.

The first discharge curves of the obtained $LiMn_2O_4$ and Li_2MnO_3 are shown in Figure 5a and b. The initial discharge capacity of single crystalline $LiMn_2O_4$ at 0.1C is 124.5 mAh g^{-1} in Figure 5a. The discharge curves show two close pseudo plateaus: the extraction of Li^+ ions from one half of the tetrahedral sites with Li-Li interaction at 4.05 V (vs. Li/Li^+) and that from the other half of the tetrahedral sites without Li-Li interaction at 4.17 V (vs. Li/Li^+), which agrees with the literature.[17] Figure 5b shows the initial discharge curve for the electrodes made from Li_2MnO_3. Li_2MnO_3 electrodes have larger initial discharge capacity (327.6 mAh g^{-1}). The reason is that during the process of initial charge, lithium ions in the transition metal layers diffuse into the lithium-depleted layers to provide sufficient binding energy in order to maintain the integrity of the close-packed oxygen array,[18] which enhanced the discharge capacity of the electrode.

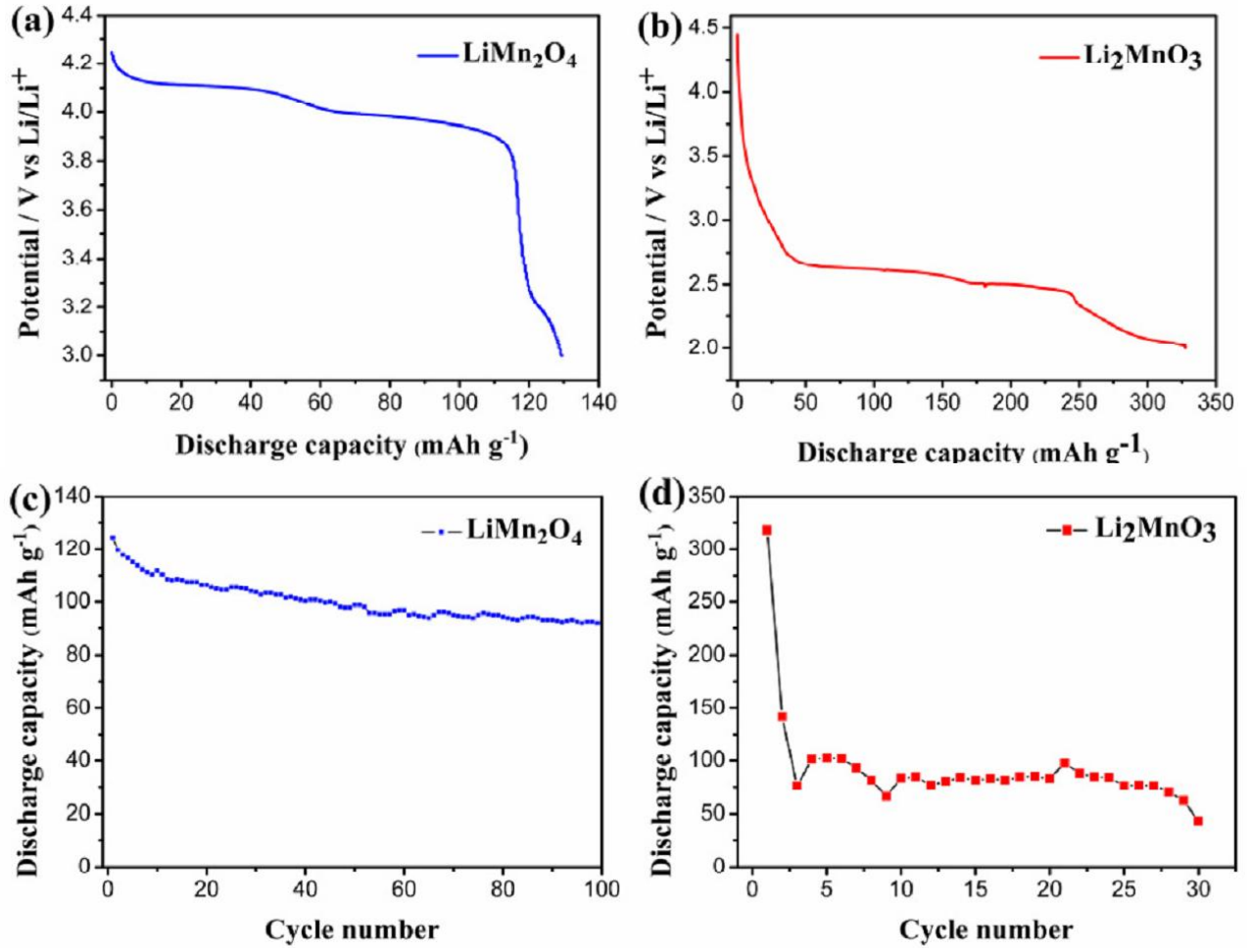

Figure 5. Initial discharge curves of the obtained materials at 0.1C (a) $LiMn_2O_4$ and (b) Li_2MnO_3, (c) the cycling stability curve of $LiMn_2O_4$ electrodes between potential limits of 3.0 and 4.3V at the 0.1C rate, and (d) the cycling stability curve of Li_2MnO_3 electrodes between potential limits of 2.0 and 4.6V at the 0.1C rate.

Figure 5c and d showed the cycle performance of the as-synthesized $LiMn_2O_4$ electrodes and Li_2MnO_3 electrodes at the 0.1C rate, respectively. The discharge capacity of $LiMn_2O_4$ shows very

good capacity retention as one can observe in Figure 5c. The initial discharge capacity and average discharge capacity of the current rate of 0.1 C are around 124.5 mAh g^{-1} and 105.9 mAh g^{-1}, respectively. By the way, the $LiMn_2O_4$ behaved a quite slow capacity fading on cycling with an average capacity loss of 0.023 mAh g^{-1} per cycle during 100 charge-discharge cycles. Although the first coulombic efficiency of the electrode is only 95%, caused by the solid electrolyte interphase (SEI) formation and other Li-consuming surface reactions during the first charge/discharge cycling,[19] the subsequent coulombic efficiency reaches nearly 100%. Figure 5d showed the cycle performance of the as-synthesized Li_2MnO_3 electrodes at the 0.1C rate. Although the initial discharge capacity for Li2MnO3 is 327.6 mAh g^{-1}, the irreversible capacity loss is much more and the capacity retention is only 16% after 20 cycles.

4. CONCLUSIONS

In summery, we have successfully fabricated Li-Mn-O compounds by solid state reaction using γ-MnOOH nanorods as a self-template. It is found that the crystal structure of Li-Mn-O can be changed from $LiMn_2O_4$ (Fd3m) to Li_2MnO_3 (C2/m) as Li content increases. Besides, electrochemical tests manifest that $LiMn_2O_4$ has excellent advantages over cycling performance and discharge capability. More importantly, the synthetic method presented here may also provide a general strategy for the fabrication of other Li-Mn-O compounds.

ACKNOWLEDGEMENTS
This work was supported by the National Science & Technology Pillar Program (2012BAK04B09).

References

1. B. Scrosati, *Nature* 373 (1995) 557.
2. S.Y. Chung, J.T. Bloking, Y.M. Chiang, *Nat. Mater.* 1 (2002) 123.
3. K.S. Kang, Y.S. Meng, J. Breger, C.P. Grey, G. Ceder, *Science* 311 (2006) 977.
4. A. Manthiram, A. VadivelMurugan, A. Sarkar, T. Muraliganth, *Eng. Environ. Sci.* 1 (2008) 621.
5. M. Jayalakshmi, M.M. Rao, F. Scholz, *Langmuir* 19 (2003) 8403.
6. J. Cabana, T. Valdes-Solis, M.R. Palacin, J. Oro-Sole, A. Fuertes, G. Marban, A.B. Fuertes, *J. Power Sources* 166 (2007) 492.
7. J.Y. Luo, Y.G. Wang, H.M. Xiong, Y.Y. Xia, *Chem. Mater.* 19 (2007) 4791.
8. M.M. Thackeray, C.S. Johnson, J.T. Vaughey, N. Li, S.A. Hackney, *J.Mater.Chem.* 15 (2005) 2257.
9. E.M. Jin, B. Jin, Y.S. Jeon, K.H. Park, H.B. Gua, *J. Power Sources* 189 (2009) 620.
10. J.Y. Luo, H.M. Xiong, Y.Y. Xia, *J. Phys. Chem. C* 112 (2008) 12051.
11. P. Sang-Ho, S. Yuichi, K. Jae-KooK, L. Yun-Sung, *Mater. Chem. Phys.* 102 (2007) 225.
12. W.X. Zhang, Z.H. Yang, Y. Liu, S.P. Tang, X.Z. Han, M. Chen, *J. Cryst. Growth* 263 (2004) 394.
13. T. Kohler, T. Armbrustor, E. Libowitzky, *J. Solid State Chem.* 133 (1997) 486.
14. K. Pramod, M.S. Sharma, Whittingham, *Mater.Lett.* 48 (2001) 319.
15. T.F. Yi, C.L. Hao, C.B. Yue,R.S. Zhu, J. Shu, *Synth. Met.* 159 (2009) 1255.

16. J. Bregér, M. Jiang, N. Dupre, Y.S. Meng, Y. Shao-Horn, G. Ceder, C.P. Grey, *J. Solid State Chem.* 178 (2005) 2575.
17. M.M. Thackeray, W.I.F. David, P.G. Bruce, J.B. Goodenough, *Mater. Res. Bull.* 18 (1983) 461.
18. K. Kang, G. Ceder, *Phys. Rev. B* 74 (2006) 094105-1.
19. S Y.G. Guo, J.S. Hu, L.J. Wan, *Adv. Mater.* 20 (2008) 2878.